Fundamental study of crystallization, orientation, and electrical conductivity of electrospun PET/carbon nanotube nanofibers

Mazinani, Saeedeh; Ajji, Abdellah; Dubois, Charles

Publisher's version / Version de l'éditeur:
https://doi.org/10.1002/polb.22085
Journal of Polymer Science. Part B, Polymer Physics, 48, 19, pp. 2052-2064, 2010-10-01

NRC Publications Record / Notice d'Archives des publications de CNRC:
https://nrc-publications.canada.ca/eng/view/object/?id=dc1539d4-7e23-4169-868d-97c7c6b34461
https://publications-cnrc.canada.ca/fra/voir/objet/?id=dc1539d4-7e23-4169-868d-97c7c6b34461

Fundamental Study of Crystallization, Orientation, and Electrical Conductivity of Electrospun PET/Carbon Nanotube Nanofibers

SAEEDEH MAZINANI,[1] ABDELLAH AJJI,[1,2] CHARLES DUBOIS[1]

[1]CREPEC, Department of Chemical Engineering, Ecole Polytechnique de Montreal, P.O. Box 6079, Station Centre-Ville, Montreal, Quebec, Canada H3C 3A7

[2]CREPEC, Industrial Materials Institute, National Research Council Canada, 75, de Mortagne, Boucherville, Quebec, Canada J4B 6Y4

Received 10 June 2009; revised 2 March 2010; accepted 6 June 2010
DOI: 10.1002/polb.22085
Published online in Wiley Online Library (wileyonlinelibrary.com).

ABSTRACT: The morphology, structure, and properties of polyethylene terephthalate (PET)/Carbon Nanotubes (CNT) conductive nanoweb were studied in this article. Nanocomposite nanofibers were obtained through electrospinning of PET solutions in trifluoroacetic acid (TFA)/dichloromethane (DCM) containing different concentrations and types of CNTs. Electrical conductivity measurements on nanofiber mats showed an electrical percolation threshold around 2 wt % multi-wall carbon nanotubes (MWCNT). The morphological analysis results showed smoother nanofibers with less bead structures development when using a rotating drum collector especially at high concentrations of CNTs. From crystallographic measurements, a higher degree of crystallinity was observed with increasing CNT concentrations above electrical percolation. Spectroscopy results showed that both PET and CNT orientation increased with the level of alignment of the nanofibers when the nanotube concentration was below the electrical percolation threshold; while the orientation factor was reduced for aligned nanofibers with higher content in CNT. Considerable enhancement in mechanical properties, especially tensile modulus, was found in aligned nanofibers; at least six times higher than the modulus of random nanofibers at concentrations below percolation. The effect of alignment on the mechanical properties was less important at higher concentrations of CNTs, above the percolation threshold. © 2010 Wiley Periodicals, Inc. J Polym Sci Part B: Polym Phys 48: 2052–2064, 2010

KEYWORDS: carbon nanotubes; crystallization; electrospinning; fibers; nanocomposites; orientation

INTRODUCTION The electrospraying process was discovered by Formhal (1934) and since then, this process has received a great deal of interest due to its apparent simplicity.[1] Electrospinning is the most practical technique to produce nanofibers. Until 1993, the electrospinning technology was often referred to as an electrostatic spraying process and only a few publications employing this technique can be found prior to that year.[2] Reneker and Chun revisited this technology in the 1990s, and they showed the possibility of using it for producing nanofibers from several types of polymer solutions.[3] More recently, composites nanofibers were obtained by dispersing various types of nanoparticles in these polymer solutions and thus, the nanoparticles were embedded in the nanofibers during the electrospinning process. While several types of particles have been studied, among them, carbon nanotubes (CNTs) have received a particular attention. In fact, rapidly after their development,[4] CNTs have been widely used to improve electrical or mechanical properties of electrospun polymer nanofibers.[5–8] The presence of CNTs enhances the conductivity of the polymer solution and produces a larger electrical current during electrospinning. The addition of charge accumulation overcomes cohesive forces and intensifies repulsive forces among the charges accumulated inside nanofibers and fibers of smaller diameter are formed.[6]

Several researchers investigated the structures, properties and applications of polyethylene terephtalate (PET) electrospun nanofibers with and without CNT.[9–24] Considering the unique properties of PET, various applications of PET nanofibers have been developed.[9–11,13,15,16,18–23] These include filtration,[9,16,19,20] phase change materials (PCM),[10,13] charge storage,[11] and biomedical applications.[15,18,21,22] However, very few studies addressed with a satisfactory level of details the structure and properties of PET nanofibers produced by solution electrospinning. The earliest one was performed by Kim et al., who investigated the electrospinning of PET with an emphasis on the effect of molecular weight and linear velocity of the collecting drum surface.[24] They used X-ray diffraction (XRD) to assess the effect of drum velocity on nanofibers orientation and the resulting crystallinity.[24] McKee et al. studied the correlation between

Correspondence to: C. Dubois (E-mail: charles.dubois@polymtl.ca)

solution rheology and final nanofiber morphologies of branched and linear polyester electrospun nanofibers.[23] They found that the concentration required for bead-free nanofiber production is two times more than c^* (the concentration required for chain entanglement initiation). The effect of chain entanglements on viscosity was also studied, and a correlation of the electrospun morphology (polymer droplets, beaded structure, or nanofibers) to zero shear rate viscosity was developed.[23] In one of the most recent studies available on the production of PET nanofiber by electrospinning, Veleirinho and his colleagues evaluated the effect of initial solution concentration and solvent type on final properties of PET electrospun nanofibers.[14] They showed that at least 10 wt % of PET is required to prepare nanofibers, while higher concentration favors beadless structure nanofibers.[14] They also showed that in the composition of the solvents mix, TFA/DCM volume ratio could be an important determining factor on the final morphology and properties of nanofibers.[14] In one of the earliest works available, polybutylene terephthalate (PBT), a polyester similar to PET and CNT were combined and electrospun to fibers.[25] A suspension of 5 wt % MWCNT dispersed in a solution of PBT/hexafluoro isopropanol (HIFP) produced fibers with an improved thermal stability and better mechanical properties.[25] More recent studies on structure and properties of PET/CNT nanocomposite nanofibers are also found in refs. 26 and 27. In 2008, Ahn et al. investigated the properties of PET/MWCNT nanocomposite nanofibers for the first time.[26] They improved the dispersion of 3% w/w or less MWCNT suspensions by an acid treatment on the nanotubes to increase the amount of chemical groups at their surface. Morphology, physical, and mechanical properties of the resulting nanofibers were studied; however, the electrical conductivity did not improve significantly.[26] In the most recent work available on PET/MWCNT nanocomposite nanofibers, the molecular conformation structure and chain orientation of PET in nanocomposite nanofibers after electrospinning has been studied by Chen et al.[27] They investigated the effect of MWCNT addition on PET chain confinement at different concentrations, up to 2 wt % MWCNT, by differential scanning calorimetery (DSC) and FTIR techniques. They mainly studied the crystallinity and morphology of PET fibers with and without MWCNT.[27] However, they did not report any data about the final electrical and mechanical properties of their nanocomposite electrospun nanofibers.

In the present study, PET solutions containing different types and concentrations of carbon nanotubes (single-wall, double-wall, and multi-wall) are electrospun to produce nanocomposite nanofibers. The effect of CNT addition on nanofiber morphology is studied both quantitatively and qualitatively. We mainly focus on final nanofibers and mats characteristics at a wide range of MWCNT concentrations, and especially at high concentrations of CNTs. Moreover, aligned nanofibers are produced by using a rotating drum. DSC, FTIR, and Raman spectroscopy are employed to characterize the properties of nanocomposite nanofibers obtained with a static collection mode as compared with those obtained from a rotating receptor. In addition, electrical conductivity and mechanical properties of the resulting nanowebs at different CNT contents and types are obtained. The extensive use of PET by the fiber and textile industry motivates our efforts towards the production of conductive nanocomposite nanofibers mat by electrospinning. Such an extensive characterization of PET/CNT composites nanofibers produced for a large variety of CNT concentrations and types and under several processing conditions is, to the best of our knowledge, reported for the first time.

EXPERIMENTS

Polymer Solution Preparation and Electrospinning Process

The polymer used in this work was a polyethylene terephthalate with IV = 1 (Selar 7086, DuPont Co.), dissolved at 10% w/w concentration in an equal volume mixture of trifluoroacetic acid (TFA) and dichloromethane (DCM); both solvents were purchased from Aldrich Co. Carbon nanotubes produced by a chemical vapor deposition process (CVD) were purchased from Helix Co. (Richardson, Texas). Single wall carbon nanotubes (SWCNT) and double wall carbon nanotubes (DWCNT) with purities of 90 wt % and multi wall carbon nanotubes (MWCNT) with purity of 95 wt % were procured. The nominal diameter ranges of SWCNT, DWCNT, and MWCNT were, respectively, of 1.3 nm, 4 nm, and 10–100 nm. All three types of CNT had lengths in the range of 0.5–40 μm. CNTs at different concentrations were dispersed mechanically in pure TFA by a 2 h sonication treatment at room temperature followed by continuous mechanical mixing (by a stirrer in a container). The mixture was sonicated an additional 2 h after addition of PET and DCM and complete dissolution of PET by continuous stirring. Final suspensions were stirred continuously before electrospinning. No surface modification technique was employed to prevent its detrimental effect on the electrical conductivity of the CNTs.

Electrospinning Process

The electrospinning set-up employed in this work consisted in a high voltage power supply (Gamma), a syringe pump to deliver the solution at specific flow rates (PHD 4400, Harvard Apparatus), a syringe connected to a stainless steel needle (22 gauge, Popper and Sons), and finally a stainless steel collecting drum (15 cm diameter). Nanofiber mats were collected in both static and rotating drum conditions (to obtain aligned nanofibers by rotating drum). An average electrical potential difference of 10 kV was used on all types of materials. The voltage was imposed on the needle, positioned at a 15 cm distance from the collector and a volumetric flow rate of 0.5 mL/h was maintained. All experiments were conducted at ambient pressure and temperature in a relative humidity environment of 20% in average. A summary of the different carbon nanotube concentrations and types studied here, and the resulting nanofibers diameter and morphology is given in Table 1. In the case of aligned nanofibers production, we used a drum (of 150 mm

TABLE 1 Summary of the Produced Nanocomposite Nanofibers and Their Resulting Characteristics at 10% w/v Concentration of PET

CNT Type and Concentration	Collecting Method	Resulting Morphology	Average Fiber Diameter (nm)
0 wt % MWCNT	Static drum	Random smooth beadless fibers	1008 ± 137
0 wt % MWCNT	Rotating drum	Aligned smooth beadless nanofibers	827 ± 195
1 wt % MWCNT	Static drum	Random smooth beadless nanofibers	495 ± 74
1 wt % MWCNT	Rotating drum	Partially aligned smooth beadless nanofibers	966 ± 228
2 wt % MWCNT	Static drum	Random smooth beadless nanofibers	–
3 wt % MWCNT	Static drum	Random nanofibers; including small beads	481 ± 78
3 wt % MWCNT	Rotating drum	Partially aligned smooth beadless nanofibers	591± 152
4 wt % MWCNT	Static drum	Random nanofibers; including large beads	–
5 wt % MWCNT	Static drum	Random nanofibers; including large beads	388 ± 84
5 wt % MWCNT	Rotating drum	Partially aligned smooth beadless nanofibers	447 ± 135
1 wt % SWCNT	Static drum	Random smooth beadless nanofibers	497 ± 100
5 wt % SWCNT	Static drum	Random nanofibers; including large beads	445 ± 137
1 wt % DWCNT	Static drum	Random nanofibers; including small beads	550 ± 137
5 wt % DWCNT	Static drum	Random nanofibers; including large beads	463 ± 98

in diameter) rotation speed of 600 rpm and the same electrospinning parameters as mentioned previously.

Morphological Analysis and Evaluation of CNTs

A Hitachi *S*-4700 scanning electron microscopy (SEM) was used on platinum coated samples to characterize the final morphologies and surface structures of nanofibers at different processing conditions and CNT concentrations. Two other techniques, high-resolution scanning electron microscopy (HR-SEM) and transmission electron microscopy (TEM) were also employed to study final nanofibers morphologies and surface structure (by HR-SEM) and CNT localization in nanofibers (by TEM). Moreover, an optical microscope, Dialux 20 (Leitz, WETZLAR), was employed to assess the dispersion condition and CNTs position inside nanofibers.

Crystalline Characteristics (DSC and XRD)

DSC and XRD were used to study the crystalline behavior of PET/CNT nanocomposite nanofibers. The effect of CNT addition on crystalline structure and behavior of nanofibers was first investigated by differential scanning calorimetry (DSC, Q1000; TA Instruments). The tests were performed in non-isothermal condition and included a heating/cooling/heating cycle with the rate of 10 °C/min. The crystallinity of the polymer was further studied with X-ray diffraction (XRD, Discover, D8, Bruker) using the X-ray goniometer accompanied with a Hi-STAR two-dimensional area detector. The generator voltage and current were 40 kV and 40 mA, respectively, and the Cu Kα radiation ($\lambda = 1.542$ E) was selected by a graphite crystal monochromator. The nanofibers obtained were also examined using wide angle X-ray diffraction (WAXD) method.

Orientation Measurements (Raman and FTIR Spectroscopy)

Raman and Fourier transform infrared (FTIR) spectroscopy techniques were used for CNT and PET/CNT nanofibers orientation measurements. A Nicolet Magna 860 FTIR instrument from Thermo Electron Corp. (DTGS detector, resolution 4 cm^{-1}, accumulation of 128 scans) was employed for a quantitative evaluation of PET chains orientation in nanofibers at different MWCNT concentrations. Raman spectroscopy of the technique of choice for CNT quantitative orientation measurements. Raman spectra were recorded on a Renishaw spectrometer equipped with an inVia Raman microscope. The samples were tested using a NIR laser (785 nm) with a grating of 1200 g/mm in a regular mode and use of 50×, short working distance (SWD) microscope. Orientation of MWCNTs was obtained by comparing the spectra in directions parallel and perpendicular to the laser beam in aligned nanofibers.

Electrical Conductivity

Electrical conductivity of final nanowebs was measured using various instruments. The system becomes conductive when a critical concentration is reached which is called the electrical percolation threshold, above which the system is quite conductive. In the case of high resistance materials (below percolation), a KEITLEY 6517, high resistance meter was used, and in the conductive range (above percolation) a combined set-up of KEITHLEY 6620 as a current source and Agilent 34401 A (6 [1/2] Digit Multimeter) as voltage source were used.

Mechanical Properties

The mechanical properties of nanowebs produced with different CNT types and concentrations were obtained with the help of a micro-tester 5548 (Instron). The tensile test was performed using a 5*N* load cell and a speed of 10 mm/min on nanofibers mats varying from 20 μm to 150 μm in thickness. Even though each concentration included samples

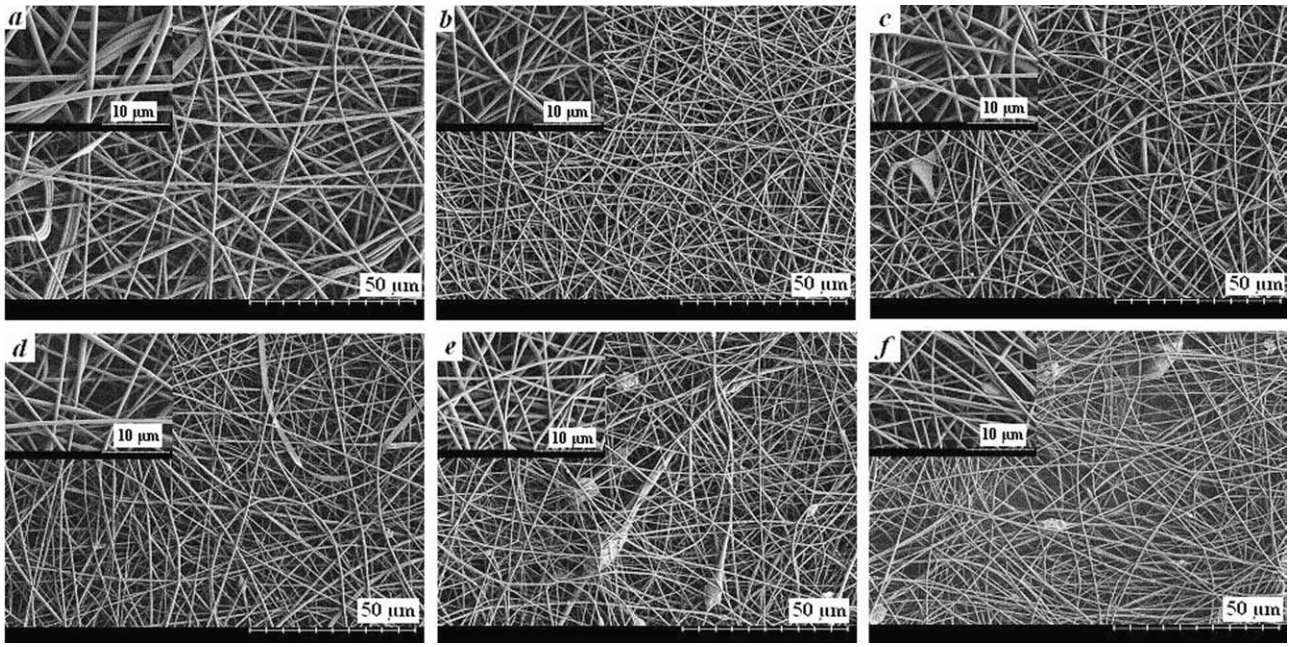

FIGURE 1 SEM photos of PET (10 wt %)/MWCNT at different CNT concentrations. (a) Pure PET; (b) 1 wt % MWCNT; (c) 2 wt % MWCNT; (d) 3 wt % MWCNT; (e) 4 wt % MWCNT; (f) 5 wt % MWCNT.

of different thickness, the average thickness was kept almost constant for all types of samples.

RESULTS AND DISCUSSIONS

Morphological Analysis and Dispersion Evaluation

A morphological study of electrospun nanofibers at different conditions was first performed. PET/CNT nanocomposite nanofibers at different MWCNT concentrations were produced and collected as randomly shaped nanofibers on a static drum (Fig. 1 and Table 1). The results show that nanofibers have almost the same normal and narrow distribution of diameters (Table 1). The average nanofiber diameter of pure electrospun nanofibers ($\sim$1 μm) is greatly reduced by adding only 1 wt % MWCNT [Fig. 1(b)]. This is attributed to the increase in the conductivity of the solution upon addition of MWCNT.[6] A change in the level of dispersion of MWCNT in the initial solution causes a large decrease in average nanofiber diameter even at 1 wt % MWCNT. The results show that the average nanofiber diameter decreases gradually to a final diameter of about 400 nm at 5 wt % MWCNT concentration (Table 1); this reduction is interpreted as due to the increase in the conductivity of electrospinning solution. Below 3 wt % MWCNT, smooth and beadless nanofiber structures are obtained. At 3 wt % MWCNT small beads start to develop in spite of the fact that there is still a reduction in final nanofiber diameter [Fig. 1(d)]. The small beads at 3 wt % MWCNT become larger at the higher MWCNT concentration of 4 and 5 wt % [Fig. 1(e,f)].

The effect of replacing the MWCNTs by two other types of CNTs (SWCNT, DWCNT) at low (1 wt %) and high (5 wt %) concentrations was also studied. A similar nanofiber structure is obtained for all types of CNTs including almost the same range of nanofiber diameter. Some bead structures developed and the nanofibers are less smooth at 1 wt % DWCNT (Table 1) as compared to the other types of CNTs. Moreover, the average final nanofiber diameter also increased for this system (Table 1). At 5 wt % CNT, the same range of nanofiber diameter is obtained for all types of CNTs (Table 1). Moreover, they all include bead structures formation along nanofiber axis (Table 1). All the beads showed a rough surface structure as showed in Figure 2 using optical microscopy [Fig. 2(a)] and high resolution SEM [Fig. 2(b)]. At high concentrations of carbon nanotubes (above 3 wt %), large aggregates are observed along nanofiber axis and especially at bead positions [Fig. 2(a)]. HR-SEM (high resolution SEM) image of the beads and beads surface [Fig. 2(b)] shows the CNT position at bead surface. Therefore, there are aggregates both inside the beads and at bead surfaces of the nanocomposite nanofibers.[28]

The surface morphology of the beads along nanofiber axis at 5 wt % SWCNT and 5 wt % DWCNT, was also investigated using HR-SEM technique (Fig. 3). As it is shown, aggregates of carbon nanotubes at bead positions and close to the surfaces of the bead structures bring more roughness to the surface of the nanofibers at bead positions compared to other locations along nanofiber axis. The roughness at bead positions is probably due to aggregated CNTs close to the surface of the nanofibers; while the orientation and alignment of carbon nanotubes along nanofiber axis reduces the aggregates formation. Therefore, aggregate formation at high concentrations of carbon nanotubes changes both nanofibers morphologies (increasing bead formations, Fig. 2) and final surface topologies (increasing roughness, Fig. 3) of

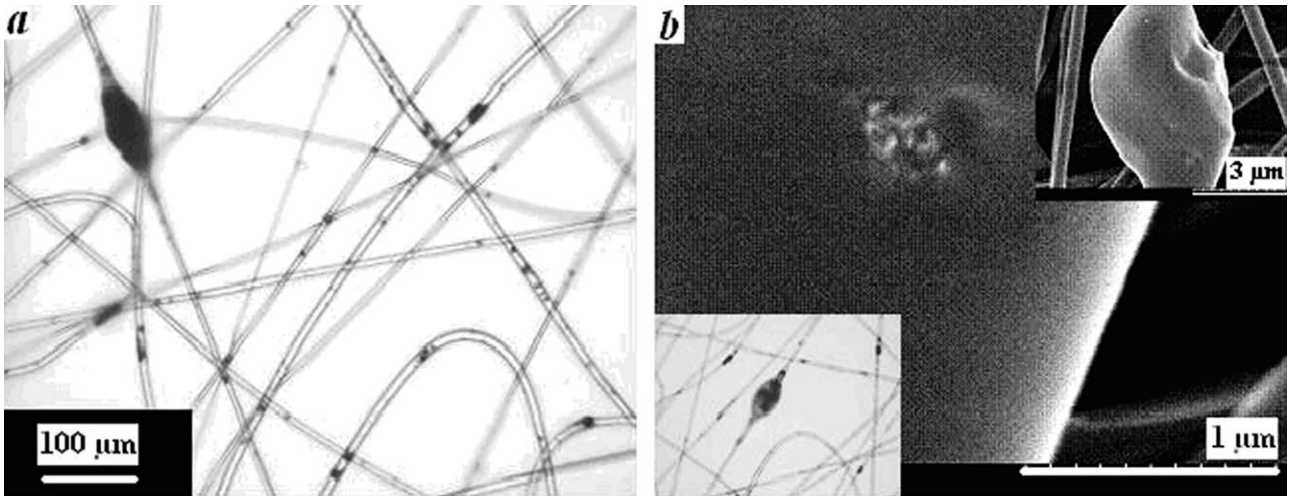

FIGURE 2 CNT localization inside nanofibers and at nanofibers surface; PET (10 wt %)/MWCNT (3 wt %); (a) optical microscopy; (b) SEM.

nanocomposite nanofibers. TEM method was used to study the relative position of CNTs inside the nanocomposite nanofibers (Fig. 4). TEM images of nanofibers along nanofiber axis [Fig. 4(a)] and at nanofiber cross section [Fig. 4(b)] show formation of CNTs small aggregates which confirms the SEM observations. In addition, it is possible to detect single oriented carbon nanotube along nanofiber axis [Fig. 4(c)] after electrospinning.

We used the same processing conditions mentioned previously but with a rotating drum to obtain aligned nanofibers and to compare the results with nanofibers collected on static drum. All electrospun samples were quite well aligned macroscopically; however, using SEM observations, it was found that pure PET electrospun nanofibers were more aligned, which is in agreement with the reduction in average nanofiber diameter of aligned PET nanofibers to about 800 nm (Table 1). The SEM pictures show that it is possible to obtain an oriented nanofiber structure in pure PET electrospun nanofibers [Fig. 5(a)] and partially aligned nanofibers after adding MWCNT [Fig. 5(b–d)].

The reduction in diameter for aligned nanofibers has also been reported by Fenessey and Farris.[29] As opposed to what could be expected in light of previously reported data on pure PET aligned nanofibers,[30] the average nanofiber diameter is increased by adding carbon nanotubes in aligned nanocomposite nanofibers (see Table 1). The increase in average nanofiber diameter is maximum at 1 wt % MWCNT; however, this effect is also observed at 3 wt % and 5 wt % MWCNT, but to a lesser extent. In addition, the aligned nanocomposite nanofibers present a wider diameter distribution.

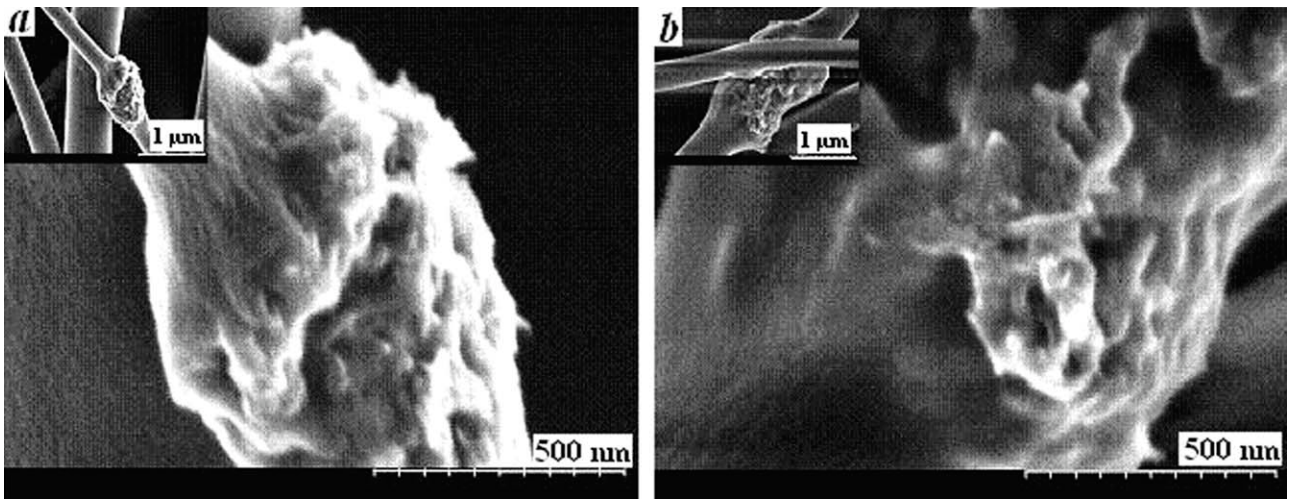

FIGURE 3 HR-SEM photos of surface topology of bead structures at high CNT concentrations. (a) PET (10 wt %)/SWCNT (5 wt %); PET (10 wt %)/DWCNT (5 wt %).

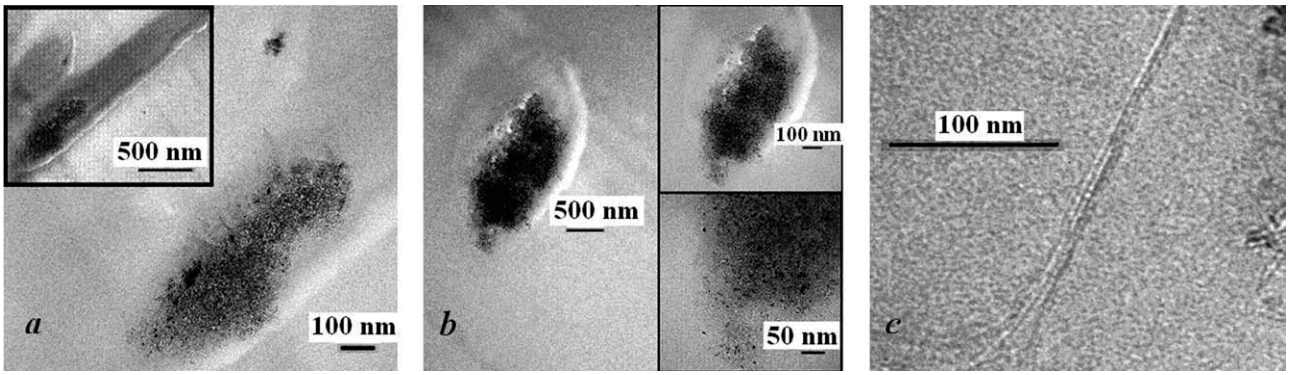

FIGURE 4 TEM photos of CNT localization in PET/MWCNT (3 wt %) electrospun nanofibers; (a) CNT aggregates along nanofiber axis; (b) CNT aggregates across nanofiber; (c) single CNT along nanofiber axis.

The observations on aligned nanocomposite nanofibers show that there are less large beads along nanofiber axis as compared to random nanofibers of equal CNT concentrations. Aligned nanocomposite nanofibers include less bead structures, and their size is also decreased. We believe that at high concentrations of carbon nanotubes, the electrical forces are preferentially applied on carbon nanotubes rather that polymer matrix; therefore, more smooth nanofibers with larger diameters are obtained.[6] The effects of CNT on orientation and after alignment will be discussed in more detailed in the next sections of this article.

Crystalline Characteristics (DSC and XRD)

The crystalline structure of nanocomposite electrospun nanofibers and the role of CNT addition are important parameters in controlling their final properties. The effect of CNT addition on PET/CNT electrospun nanocomposite nanofibers was first studied by the DSC technique and then by X-ray diffraction.

DSC Results

The values of ΔH used in different calculations and for DSC analysis reported here have been corrected for nanoparticles content by the following equation to have the data purely related to polymer weight:

$$\Delta H_{\mathrm{i,corrected}} = \Delta H_{\mathrm{i,experiment}}/(1 - w_{\mathrm{CNT}}) \quad (1)$$

Then, the degree of crystallinity was calculated by the following equation[31]:

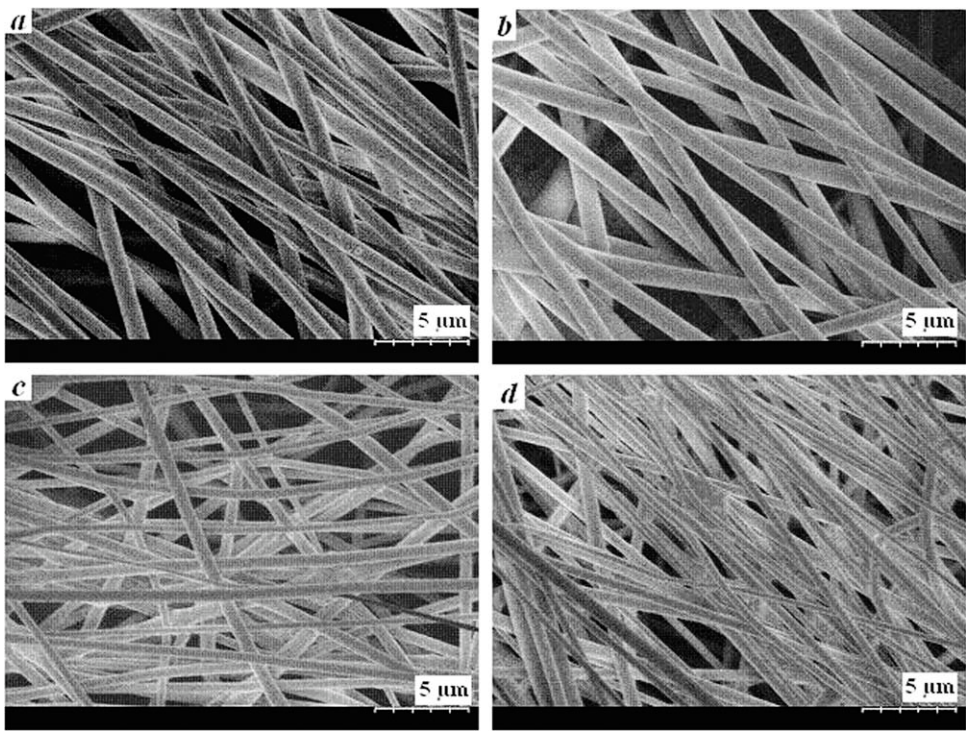

FIGURE 5 SEM photos of aligned PET (10 wt %)/MWCNT at different CNT concentrations. (a) Pure PET; (b) 1 wt % MWCNT; (c) 3 wt % MWCNT; (d) 5 wt % MWCNT.

TABLE 2 Thermal Parameters of Nanocomposite Nanofiber Mats at Different CNT Concentrations and Types

	T_g (°C)	Crystalline Content of Electrospun Nanofibers (%)	$\Delta H_{\text{first-heating}}$ (J/g)	$\Delta H_{\text{second-heating}}$ (J/g)
Pure PET	76.7	15.6	42.6	41.1
PET/1 wt % MWCNT	75.4	14.3	39.7	38.6
PET/2 wt % MWCNT	75.5	9.4	38.7	38.3
PET/3 wt % MWCNT	76.3	13.6	35.7	33.9
PET/4 wt % MWCNT	77.8	14.4	35.6	33.6
PET/5 wt % MWCNT	79.0	15.1	35.7	33.9
PET/1 wt % SWCNT	81.6	13.2	33.0	28.3
PET/5 wt % SWCNT	81.9	14.1	30.6	28.5
PET/1 wt % DWCNT	79.9	10.8	33.1	30.6
PET/5 wt % DWCNT	81.2	13.0	35.5	29.6

$$X_c = (\Delta H_f - \Delta H_{rc})/\Delta H_f^0 \quad (2)$$

where ΔH_f is the enthalpy of fusion, ΔH_{rc} is the enthalpy of re-crystallization occurring during heating cycle, and ΔH_f^0 is the enthalpy of fusion of perfectly crystalline structure of PET at equilibrium thermodynamic melt temperature T_m^0 and was taken as 140 J/g.[32]

Thermal parameters and the data obtained after a heating/cooling/heating cycle for each sample are given in Table 2. The results show first a decrease and then an increase in crystallinity as a function of CNT content. MWCNT content below 2 wt % causes a decrease in crystallinity as reported elsewhere.[27] A similar trend is also observed for the glass transition temperature T_g. However, at a MWCNT content of 3 wt % or more, an increase in crystallinity and T_g is observed. At a concentration of 5 wt % in MWCNT, the maximum crystallinity is obtained. It will be shown thereafter that the 2 wt % threshold governing the crystallization behavior of the PET based nanocomposites fibers also corresponds to the electrical percolation threshold. Crystallinity is controlled by two factors: nucleation and growth. Addition of CNT increases the number of nucleation sites;[33] however, it also decreases the rate of growth, and the chains are more inclined to be oriented rather than entering the crystalline cells.[27] Above 2 wt %, the larger amount on nucleation sites overcomes the slower crystallization kinetics and, as a result, the overall crystallinity is also increased. The data shown at 1 wt % and 5 wt % SWCNT and DWCNT exhibit the same trend as those obtained for MWCNT (Table 2). T_g is higher in the case of SWCNT and DWCNT, which might be due to their smaller size. The latter causes more interactions between CNT particles and polymer chains. As a result, the overall motion of PET chains is restricted when the sizes of nanoparticles are reduced and an increase in T_g is observed.

The differences in ΔH for the first heating cycle (after electrospinning) and the second heating cycle (from the cooled melt) is a valuable parameter to be studied and is reported in Table 2. The higher value of ΔH obtained after electrospinning is due to the effect of oriented chains in electrospun nanofibers.[31] Oriented chains produced after electrospinning make it easier for crystallization. They can enter the crystalline cells during cold crystallization and thus increases the difference between the ΔH of these two cycles. The higher the oriented chains out of crystalline cells after electrospinning, the higher this difference will be. The confined oriented chain structure below 2 wt % CNT has been reported before.[27]

The effect of aligned nanofiber structures on crystalline behavior is given in Table 3. The trend in change of crystallinity is different from that of randomly collected nanofibers. In aligned nanofibers, the crystallinity is less than the one observed on random ones for almost all CNT concentrations. The addition of MWCNT causes a gradual increase in the amount of crystallinity. In the case of aligned nanofibers, chain alignment is increased and therefore, the chains are more inclined to be oriented rather than entering crystalline cells. That is the main reason for the change in ΔH in the first and second heating cycles as mentioned previously. A more precise study of the CNT and PET chain orientations will be discussed in more detailed in the FTIR part.

X-Ray Diffraction Characteristics

XRD diffraction results of nanofiber mats at different CNT concentrations and types showed an almost amorphous behavior for PET/CNT electrospun nanofibers [Fig. 6(a,b)]. This is in agreement with DSC results, since the crystalline content of nanocomposite electrospun nanofibers is low and therefore it is not possible to be detected in XRD. However, at 5 wt % MWCNT concentration, a weak crystalline pattern is observed [Fig. 6(c)]. This halo observed for 5 wt % MWCNT electrospun nanofiber is due to the peak positioned at $2\theta = 18^\circ$ of PET.[34] This shows that at 5 wt %, a crystalline structure begin to form in contrast with other concentrations and CNT types.

TABLE 3 Thermal Parameters of Aligned Nanofiber Mats at Different MWCNT Concentrations

Aligned Nanofiber Mats	T_g (°C)	Crystalline Content of Electrospun Nanofibers (%)	$\Delta H_{first\text{-}heating}$ (J/g)	$\Delta H_{second\text{-}heating}$ (J/g)
Pure PET	74.0	11.9	36.4	31.3
PET/1 wt % MWCNT	76.5	13.7	34.8	29.4
PET/3 wt % MWCNT	76.8	14.1	34.3	28.7
PET/5 wt % MWCNT	75.0	14.2	32.6	28.7

Orientation Detection (FTIR and Raman Spectroscopy)

For a better understanding of the polymer chains and CNT orientations, we used also FTIR and Raman spectroscopy techniques. We investigated samples at different CNT concentrations, types and alignment condition to compare the effect of each of these parameters.

FTIR Spectroscopy

Herman orientation equations are used for the evaluation of the orientation function. For an uniaxially oriented sample, the dichroic ratio D is defined as:

$$D = \frac{A_{\parallel}}{A_{\perp}} \tag{3}$$

where A is the absorbance of a specific band parallel or perpendicular to IR polarizer.[35] Then, the Herman orientation function is obtained according to[36,37]:

$$f = \frac{D-1}{D+2} \cdot \frac{2}{3\cos^2\alpha - 1} \tag{4}$$

where α is the angle between the dipole moment of a particular vibration and the chain axis. Based on the selected IR vibration, it is possible to use the Herman orientation function for calculating the amorphous or crystalline phase orientations. Here, FTIR measurements were used to assess the effect of CNT concentration and types, as well as the degree of alignment of the nanofiber structures on chain orientation.[38] PET has several characteristic absorption bands in the IR region of the EM spectrum. The most important ones are: 973 cm^{-1}: CH_2 vibration of trans conformation with $\alpha = 32°$; 1340 cm^{-1}: CH_2 wagging mode of glycol segment in trans conformation with $\alpha = 21°$; 1370 cm^{-1}: the vibration related to gauche conformation; and 1020 cm^{-1}: absorption band attributed to in-plane vibration of C—H group of benzene with $\alpha = 20°$.[35,39]

In a first step, the ratio of trans to gauche conformers (A_{1340}/A_{1370}) was employed as a means of studying the effect of CNT concentration and type on PET chains conformation in electrospun nanofibers.[27] The addition of CNTs increased the A_{1340}/A_{1370} ratio because of a simultaneous increase in trans conformation and decrease in gauche structure (Table 4). The increase in the occurrence of the trans conformation comes from the smaller nanocomposite nanofiber diameters observed in samples that contain 1 wt % of CNT. Fine nanocomposite nanofibers obtained after CNT addition are the main reason for PET chains orientation, due to the larger draw ratio. The increase in trans conformation content as shown by our FTIR results might also originate, to some extent, in the increase crystalline content of these nanofibers, as measured by DSC. This is the case in high MWCNT concentration in which the crystalline content increases; while at lower concentration of MWCNT, chain orientation is the main controlling factor as reported previously.[27] The trans to gauche conformation ratio in SWCNT and DWCNT was measured at two concentrations and similar results were obtained (Table 4). We believe that, since the size of the crystalline domains in nanocomposite nanofibers is of the same order of magnitude as their

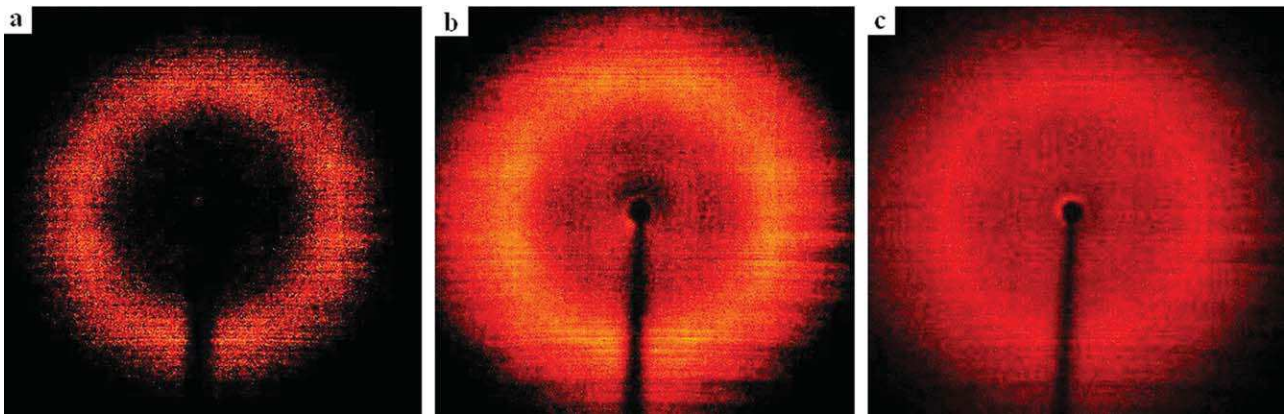

FIGURE 6 XRD pattern of PET/MWCNT electrospun nanofiber mat at different CNT concentrations; (a) pure PET; (b) PET/3 wt % MWCNT; (c) PET/5 wt % MWCNT.

TABLE 4 Relative FTIR Absorbance of Trans (1340 cm^{-1}) to Gauche (1370 cm^{-1}) Conformation (Ratio of A1340/A1370) at Different CNT Concentrations and Types of Random Nanoweb

	0 wt %	1 wt %	2 wt %	3 wt %	4 wt %	5 wt %
MWCNT	0.41	0.54	0.66	0.57	0.65	0.63
SWCNT	0.41	0.59	–	–	–	0.57
DWCNT	0.41	0.59	–	–	–	0.58

diameter, it is expected that they show an almost similar trend in the amount of orientation in random nanofibers.

The effect of nanofibers alignment on the physical and mechanical properties as compared to random nanofibers was studied here. For that purposes, samples were prepared and cut out of the mat according to Figure 7. A comparison of the values of (A_{1340}/A_{1370}) in randomly oriented nanofibers with those aligned and in parallel to the light (0°) depicts an increase in the amount of trans conformation especially in pure PET aligned nanofibers in spite of their lower crystalline density (Table 3). The results indicate that the maximum difference between the two types of fibers is obtained at 0 wt % and 1 wt % MWCNT concentration, where they are less crystalline. This could come as a proof of a higher amount of PET chains orientation at these concentrations. Quite unexpectedly, at 5 wt % MWCNT, the amount of trans to gauche conformation (A_{1340}/A_{1370}) is even more in randomly oriented nanofibers as compared to aligned. Randomly oriented nanofibers containing 5 wt % MWCNT have the larger amount of crystalline phase and the smallest nanofiber diameter. Therefore, they show the highest occurrence of the trans conformation mostly because of their more important crystalline content and not because of a more pronounced orientation of their chains. Herman orientation function (f_{1340}) measured for aligned nanofibers shows the same behavior (Fig. 8). Since the FTIR experiments were performed over final nanowebs, they do not exhibit, as one might have expected, the same high value of orientation of single nanofibers. Orientation function is reported here only to compare the amount of orientation among different aligned nanofibers containing different CNT concentrations. f_{1340} is maximum at concentrations of 0 wt % and 1 wt % MWCNT, conditions that also lead to maximum PET chains alignment and orientation as previously reported in morphological characterization.

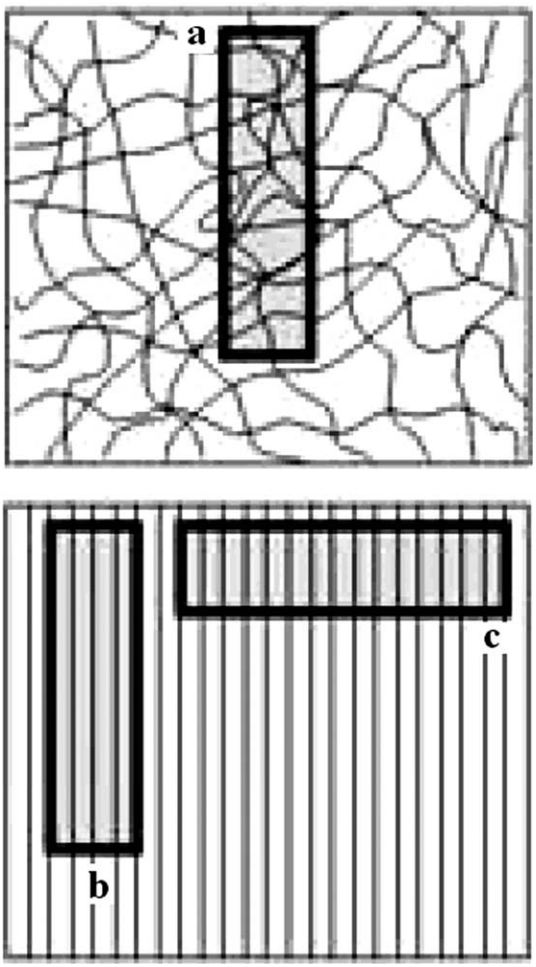

FIGURE 7 Schematic of different samples prepared and used in different experiments; (a) random nanofibers; (b) parallel to aligned nanofibers axis (0°); perpendicular to aligned nanofiber axis (90°).

Raman Spectroscopy

Among the characteristic peaks of multi-wall carbon nanotubes detected by Raman spectroscopy, three peaks could be distinguished. Two strong peaks are located at 1580 cm^{-1} (G), and 1350 cm^{-1} (D), and a weak peak is detected at around 2700 cm^{-1} (G').[40,41] D/G ratio and different peak positions of these CNTs are different based on various types of CNTs. In addition, we used the Raman spectroscopy technique for evaluating CNT orientation in aligned MWCNT/PET nanocomposite nanofibers [Fig. 9(a,b)]. As it is depicted, the spectrum reports quite different intensities in parallel and perpendicular directions [Fig. 9(a)]. The high intensities of CNT characteristic peaks found in aligned samples parallel to the beam direction indicates a high degree of alignment of

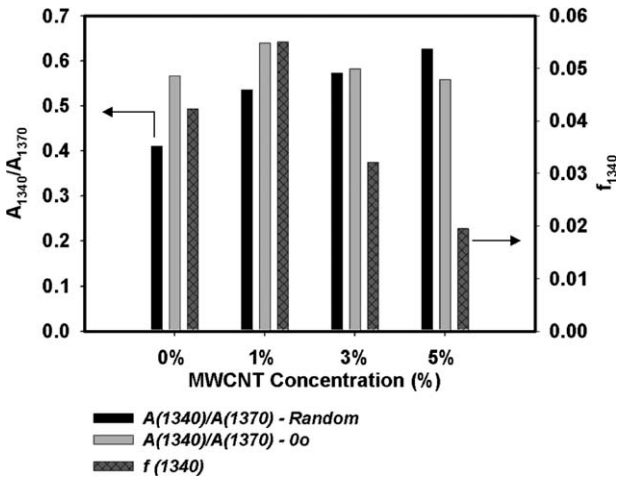

FIGURE 8 Different FTIR characteristic parameters versus MWCNT concentrations in PET/MWCNT electrospun nanofibers.

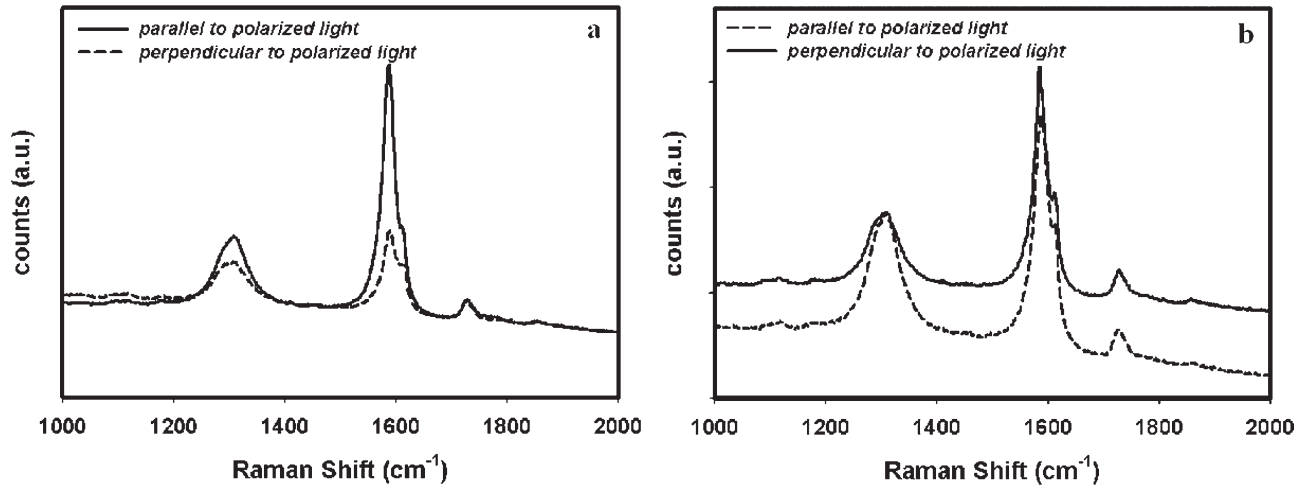

FIGURE 9 Raman spectra of aligned nanoweb parallel to polarized beam (0°) compared to perpendicular to light (90°); (a) PET/1 wt % MWCNT; (b) PET/5 wt % MWCNT.

MWCNT along the nanofiber axis. The results also prove that at 1 wt % MWCNT, quite well aligned CNTs exist inside nanofibers [Fig. 9(a)], and the beam intensity is significantly high in the parallel direction as compared to the perpendicular axis. At a concentration of 5 wt % in MWCNT, there is almost no effect of aligned nanofiber production on CNT orientation [Fig. 9(b)].

At 1 wt % MWCNT, the imposed alignment force mainly causes CNT orientation as described previously; and that is the main reason why aligned nanofibers diameter increases as compared to the static collection mode. Since the higher electric force is mostly imparted on CNTs, a retardation in splashing and diameter reduction might be expected. However, the effect of aligned nanofibers production at 1 wt % MWCNT concentration was mainly CNT orientation rather than enhancement in splashing and reduction in final nanofiber diameter. This high value of CNT orientation at 1 wt % MWCNT in aligned nanofiber manufacturing could be of considerable interest by enhancing the conductivity of single nanofibers along their axis. This is also the case with higher CNT concentrations (3 wt % and 5 wt %); alignment might be the main reason for beads removal along nanofiber axis when using the rotating drum. Alignment at high concentration mainly causes CNT bead removal rather than CNT orientation and splashing or final nanofiber diameter reduction. In conclusion, aligned nanocomposite nanofibers exhibit larger diameter at every CNT concentrations considered in this work; however, the nanofibers show more CNT orientation below percolation (1 wt % CNT) and less beads structure above percolation (3 wt % and 5 wt % MWCNT). On the other hand, higher crystallinity and lower diameter and free volume might be a reason for the observed decrease in the amount of CNT orientation at 5 wt % MWCNT. At high CNTs concentrations, large aggregates are formed inside nanofibers as shown previously. Their formation prevents the fibers from achieving a high degree of individual CNT orientation while increasing the beam intensity in the alignment direction; since it decreases the density of oriented CNTs in this direction. Hence, it might be another reason for the decrease in the amount of CNT orientation at high CNT concentrations.

Raman spectroscopy results are in agreement with both those of the SEM morphological characterization previously reported at Figure 5 and FTIR spectra shown in Figure 8. In aligned pure PET nanofibers and at 1 wt % MWCNT (below percolation), the crystalline content is low and the chains have more freedom and free volume to be oriented and therefore more aligned nanofibers are obtained below percolation based on FTIR results. Nevertheless, increase in crystallinity above percolation reduces chain movements and free volumes and therefore only a marginal PET chains orientation effect is observed in aligned nanocomposite nanofibers. This is also the case for CNT orientation in aligned nanocomposite nanofibers. At 1 wt % MWCNT, the maximum effect of aligned nanofiber processing is observed. Therefore, below the percolation threshold, aligned nanocomposite nanofibers show a very specific behavior in terms of PET chains and CNTs orientation.

Electrical Conductivity Measurements

Electrical conductivity of nanowebs of fibers was measured as a function of CNT types and concentrations. The samples included a wide range of thicknesses from 40 to 150 μm, and they were all positioned between two highly conductive layers attached to the electrodes before starting the measurements. All the experiments were run in similar conditions, giving a repeatability with a deviation of less than 15 % with respect to the average conductivity.

Based on electrical percolation theory, a system becomes conductive when a critical concentration is reached which is called the electrical percolation threshold.[42] Based on percolation theory,[43] one can express:

$$\sigma = A(w - w_c)^t \tag{5}$$

where σ is the volume conductivity, A and t are constants, and w_c is the critical concentration in which the conductivity

is very small as compared to higher concentrations. w_c can be viewed as the critical concentration for network formation (Fig. 10). As showed by the results of our conductivity measurement tests, nanofibers that contain 2 wt % of MWCNT are already quite conductive and a considerable increase in the electrical conductivity is observed after this concentration (Fig. 10). The conductivity almost reaches a plateau region above 3 wt % MWCNT concentration (Fig. 10). The electrical conductivity of nanowebs with fibers made with different types of CNTs was measured using the same method and at the same condition (Fig. 10). At 1 wt %, the conductivity is about the same for all samples, no matter the type of CNTS used. However, at 5 wt % concentration, SWCNT shows almost one order of magnitude lower conductivity compared to DWCNT and MWCNT. This might be because of fact that SWCNT were more difficult to disperse.[28]

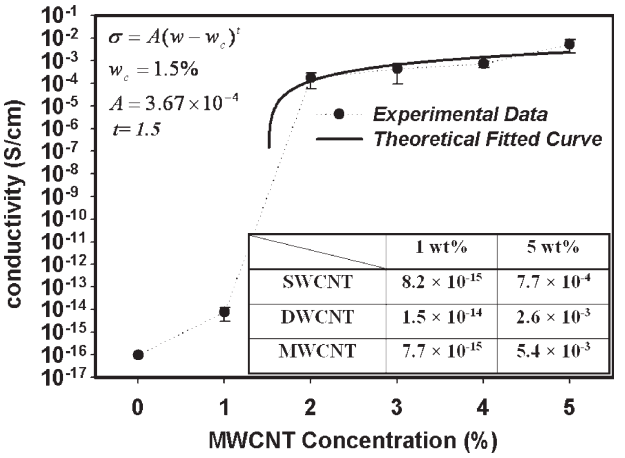

FIGURE 10 Electrical conductivity (S/cm) of nanowebs as at different CNT concentrations and types.

Mechanical Properties

Mechanical properties of electrospun PET/CNT nanofiber mats were measured at different CNTs concentrations and types.[44] Considering the results obtained, the samples containing CNTs are stronger and attain a larger elongation at break. At 1 wt % MWCNT, the nanofibers are less crystalline (Table 2); however, the chain oriented structure causes a considerable increase in ε_{break}. At 3 wt % and 5 wt %, where the samples are more crystalline (Table 2), the behavior is totally ductile in spite of these higher CNT concentrations. Crystalline formation in nanocomposite nanofibers and orientation causes an increase in modulus and strength as compared to pure PET nanowebs; while ε_{break} (Maximum tensile strain at break) is reduced with respect to nanofibers containing 1 wt % MWCNT.

Mechanical properties of randomly oriented nanofibers [Fig. 7(a)] were compared with aligned nanofibers in both parallel [Fig. 7(b)] and perpendicular [Fig. 7(c)] directions to the alignment and nanofibers orientation (Fig. 11). As it is shown, the addition of MWCNT causes an increase in modulus with respect to random PET nanofibers [Fig. 11(a)]. However, the effect of MWCNT addition on modulus in aligned nanofibers is totally opposite and it decreases in direction of the alignment (0°). The modulus for aligned mats as compared to random ones increases three to six times depending on the MWCNT concentration [Fig. 11(a)]. In samples made of random nanofibers, addition of MWCNT causes an increase in chains orientation (below percolation) and crystallinity (above percolation). Therefore for both cases, adding MWCNT increases the modulus. Samples that contained aligned nanofibers showed an increase in tensile modulus in the direction of alignment (0°). However, this effect was more important in pure PET nanofibers. By adding MWCNT, the nanofibers in the system shifts from an aligned arrangments to partially aligned distribution (Fig. 5) and therefore the modulus decreases because of a reduction in nanofibers orientation. The same trend is observed for the values of tensile strength and pure electrospun samples were the weakest specimens with random nanofibers orientation but demonstrated the highest value in aligned nanofibers in direction of alignment [Fig. 11(b)]. The difference in modulus enhancement in aligned nanofibers as compared to random mats is more important at low MWCNT concentrations. This result is consistent with FTIR and Raman spectroscopy. It has been shown in FTIR and Raman that the orientation factor of both PET chains and CNTs is maximum at low concentrations of CNTs. At high CNT concentrations, CNT aggregates, and poor dispersion could cause stress concentration and weak points in mechanical testing.

In random nanofibers, ε_{break} has a maximum value at 1 wt % MWCNT [Fig. 11(c)]. In aligned nanofibers, pure PET shows the highest value of ε_{break} and it decreases by adding MWCNT. The amount of ε_{break} for nanocomposite nanofibers is almost the same as random nanofibers and no considerable effect of alignment are observed in aligned nanocomposite nanofibers. Low modulus and strength in perpendicular direction (90°) causes considerable increase in the amount of ε_{break} especially in pure PET nanofiber mats [Fig. 11(c)].

The mechanical properties of the different nanocomposites with varying types of CNT (at 1 wt % and 5 wt %) are compared in Table 5. SWCNT and DWCNT are smaller in size and they show more compatibility with PET matrix and therefore they are more effective in mechanical properties enhancement at low concentration as compared to MWCNT. Nevertheless, the mechanical test results show opposite behavior at 5 wt % CNT concentration. This is explained by the fact that, as previously discussed, at high concentration, MWCNT are easier to disperse than SWCNT and DWCNT.[28] Dispersion has an important role on final mechanical properties, and it is quite difficult to disperse smaller sizes of nanotubes at higher concentrations.[45,46] Therefore, better results are obtained using MWCNT at high CNT concentrations.

CONCLUSIONS

Random and aligned nanocomposite nanofibers of PET with different CNTs were produced and their morphologies and

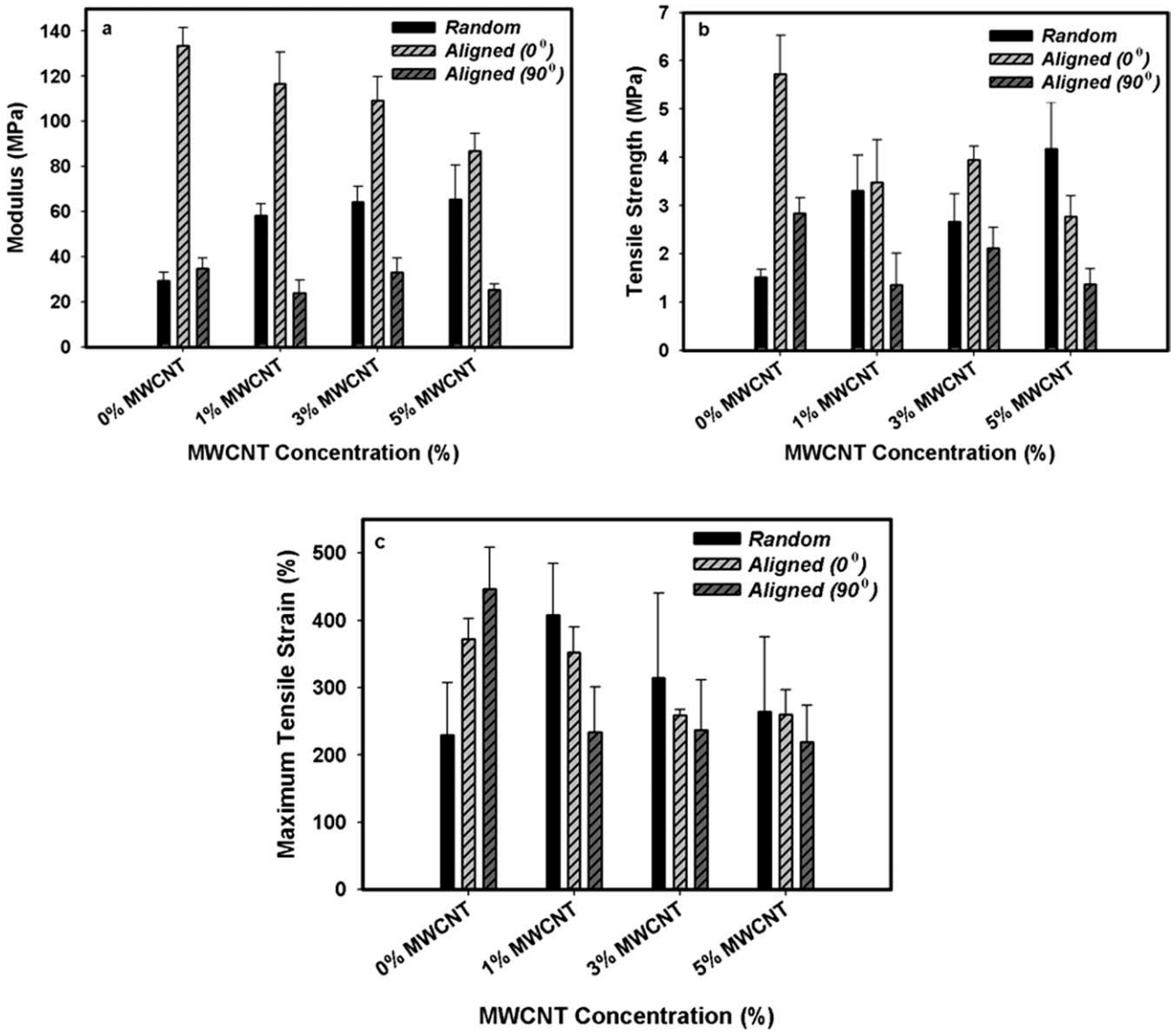

FIGURE 11 Tensile modulus (a), tensile strength (b), and maximum tensile strain (c) as a function of MWCNT concentrations in randomly oriented nanofibers compared to aligned nanofibers in parallel to alignment (0°) and perpendicular to alignment (90°).

properties studied by different methods. Electrical conductivity measurements established the percolation threshold at a concentration of 2 wt % in MWCNT. Morphological observations proved that aligned nanofibers containing MWCNT were of larger diameter but with less bead structures along the nanofiber axis. This proves that aligned nanofiber manufacturing could be useful in agglomerate reduction and smooth nanofiber production especially at high CNT concentration. Moreover, in aligned nanocomposite nanofibers, addition of CNTs caused a gradual increase in crystallinity. Therefore, it is possible to obtain nanofibers with higher crystallinity compared to random nanofibers through aligned nanofiber manufacturing at concentrations close to percolation threshold (2 wt %). It could be of considerable importance to fabricate conductive nanofibers with higher crystallinity using an aligned nanofibers production setup. The orientation of MWCNT in aligned nanocomposite nanofibers has its highest value at 1 wt % MWCNT. The maximum orientation factor obtained at 1 wt % MWCNT originates of a lesser crystalline content and more free volume available at this concentration

TABLE 5 Mechanical Properties of Nanocomposite Nanofibers Mat at Different CNT Type and Concentrations

CNT Type and Concentration	Modulus (MPa)	Tensile Strength (MPa)	Maximum Tensile Strain (%)
1 wt % SWCNT	69.0 ± 6.8	4.23 ± 0.8	315.6 ± 70.5
5 wt % SWCNT	44.9 ± 7.7	2.1 ± 0.4	148.0 ± 61.0
1 wt % DWCNT	60.0 ± 9.3	3.1 ± 0.9	256.5 ± 137.6
5 wt % DWCNT	46.5 ± 6.6	2.4 ± 0.4	264.8 ± 5.7
1 wt % MWCNT	58.3 ± 5.2	3.3 ± 0.7	408.3 ± 75.9
5 wt % MWCNT	65.4 ± 15.3	4.2 ± 1.0	264.3 ± 110.9

as compared to others. Obtaining higher orientation of CNTs at a lower concentration could help to produce more conductive single nanofiber using less CNT. Considerable effect of alignment on mechanical properties was obtained at low MWCNT concentration. Significant improvement in mechanical properties especially modulus through adding MWCNT and aligned nanofiber production could be a remarkable factor in final functionality of nanoweb.

The authors thank the financial support of Natural Sciences and Engineering Research Council Canada (NSERC) for the financial support to carry out this study. They also thank the great help of people at University of Montreal for their help in Raman spectroscopy experiments.

REFERENCES AND NOTES

1 Burger, C.; Hsiao, B. S.; Chu, B. Annu Rev Mater Res 2006, 36, 333–368.

2 Li, D.; Xia, Y. Adv Mater 2004, 16, 1151–1170.

3 Reneker, D. H.; Chun, I. Nanotechnology 1996, 7, 216–223.

4 Iijima, S. Nature 1991, 354, 56–58.

5 Ge, J. J.; Hou, H.; Li, Q.; Graham, M. J.; Greiner, A.; Reneker, D. H.; Harris, F. W.; Cheng, S. Z. D. J Am Chem Soc 2004, 126, 15754–15761.

6 Ra, E. J.; An, K. H.; Kim, K. K.; Jeong, S. Y.; Lee, Y. H. Chem Phys Lett 2005, 413, 188–193.

7 Seoul, C.; Kim, Y. T.; Baek, C. K. J Polym Sci Part B: Polym Phys 2003, 41, 1572–1577.

8 Sung, J. H.; Kim, H. S.; Jin, H. J.; Choi, H. J.; Chin, I. J. Macromolecules 2004, 37, 9899–9902.

9 Veleirinho, B.; Lopes-da-Silva, J. A. Process Biochem 2009, 44, 353–356.

10 Chen, C.; Wang, L.; Huang, Y. Sol Energy Mater Sol Cells 2008, 92, 1382–1387.

11 Ignatova, M.; Yovcheva, T.; Viraneva, A.; Mekishev, G.; Manolova, N.; Rashkov, I. Eur Polym J 2008, 44, 1962–1967.

12 Lin, Y.; Chi, L.; Yao, Y.; Wu, D. C. Iran Polym J (Eng. Ed.) 2008, 17, 373–378.

13 Chen, C.; Wang, L.; Huang, Y. Mater Lett 2008, 62, 3515–3517.

14 Veleirinho, B.; Rei, M. F.; Lopes-da-Silva, J. A. J Polym Sci Part B: Polym Phys 2008, 46, 460–471.

15 Jung, K. H.; Huh, M. W.; Meng, W.; Yuan, J.; Hyun, S. H.; Bae, J. S.; Hudson, S. M.; Kang, I. K. J Appl Polym Sci 2007, 105, 2816–2823.

16 Dotti, F.; Varesano, A.; Montarsolo, A.; Aluigi, A.; Tonin, C.; Mazzuchetti, G. J Ind Text 2007, 37, 151–162.

17 Ogata, N.; Shimada, S.; Yamaguchi, S.; Nakane, K.; Ogihara, T. J Appl Polym Sci 2007, 105, 1127–1132.

18 Chronakis, I. S.; Jakob, A.; Hagstrom, B.; Ye, L. Langmuir 2006, 22, 8960–8965.

19 Hong, K. H.; Kang, T. J. J Appl Polym Sci 2006, 100, 167–177.

20 Chronakis, I. S.; Milosevic, B.; Frenot, A.; Ye, L. Macromolecules 2006, 39, 357–361.

21 Chen, H. AIChE Annual Meeting, Conference Proceedings, American Institute of Chemical Engineers 3382–3383, New York, 2005.

22 Ma, Z.; Kotaki, M.; Yong, T.; He, W.; Ramakrishna, S. Biomaterials 2005, 26, 2527–2536.

23 McKee, M. G.; Wilkes, G. L.; Colby, R. H.; Long, T. E. Macromolecules 2004, 37, 1760–1767.

24 Kim, K. W.; Lee, K. H.; Khil, M. S.; Ho, Y. S.; Kim, H. Y. Fibers Polym 2004, 5, 122–127.

25 Nah, C.; Mathew, G.; Hong, J. P.; Rhee, J. M.; Lee, H. S. Polym Test 2005, 24, 712–717.

26 Ahn, B. W.; Chi, Y. S.; Kang, T. J. J Appl Polym Sci 2008, 110, 4055–4063.

27 Chen, H.; Liu, Z.; Cebe, P. Polymer 2009, 50, 872–880.

28 Mazinani, S.; Ajji, A.; Dubois, C. Polymer 2009, 50, 3329–3342.

29 Fennessey, S. F.; Farris, R. J. Polymer 2004, 45, 4217–4225.

30 Jose, M. V.; Steinert, B. W.; Thomas, V.; Dean, D. R.; Abdalla, M. A.; Price, G.; Janowsk, G. M. Polymer 2007, 48, 1096–1104.

31 Litchfield, D. W.; Baird, D. G. Polymer 2008, 49, 5027–5036.

32 Mehta, A.; Gaur, U.; Wundderlich, B. J Polym Sci Polym Phys Ed 1978, 16, 289–296.

33 Anoop Anand, K.; Agarwal, U. S.; Joseph, R. Polymer 2006, 47, 3976–3980.

34 Keum, J. K.; Jeon, H. J.; Song, H. H.; Choi, J. I.; Son, Y. K. Polymer 2008, 49, 4882–4888.

35 Lu, X. F.; Hay, J. N. Polymer 2001, 42, 8055–8067.

36 Cole, K. C.; Ben Daly, H.; Sanschagrin, B.; Nguyen, K. T.; Ajji, A. Polymer 1999, 40, 3505–3513.

37 Sadeghi, F.; Ajji, A.; Carreau, P. J. J Polym Sci Part B: Polym Phys 2008, 46, 148–157.

38 Lee, K. H.; Kim, K. W.; Pesapane, A.; Kim, H. Y.; Rabolt, J. F. Macromolecules 2008, 41, 1494–1498.

39 Ajji, A.; Cole, K. C.; Dumoulin, M. M.; Brisson, J. Polymer 1995, 36, 4023–4030.

40 Antunes, E. F.; Lobo, A. O.; Corat, E. J.; Trava-Airoldi, V. J. Carbon 2007, 45, 913–921.

41 Corrias, M.; Serp, P.; Kalck, P.; Dechambre, G.; Lacout, J. L.; Castiglioni, C.; Kihn, Y. Carbon 2003, 41, 2361–2367.

42 Kota, A. K.; Cipriano, B. H.; Duesterberg, M. K.; Gershon, A. L.; Powell, D.; Raghavan, S. R.; Bruck, H. A. Macromolecules 2007, 40, 7400–7406.

43 Wang, W.; Murthy, N. S.; Chae, H. G.; Kumar, S. Polymer 2008, 49, 2133–2145.

44 Inai, R.; Kotaki, M.; Ramakrishna, S. J Polym Sci Part B: Polym Phys 2005, 43, 3205–3212.

45 Coleman, J. N.; Khan, U.; Blau, W. J.; Gun'ko, Y. K. Carbon 2006, 44, 1624–1652.

46 Sluzarenko, N.; Heurtefeu, B.; Maugey, M.; Zakri, C.; Poulin, P.; Lecommandoux, S. Carbon 2006, 44, 3207–3212.